ESTIMATION OF EFFECTS OF INDENTER-TIP GEOMETRY BY MEANS OF FINITE ELEMENT ANALYSES OF NANO-INDENTATION

Satoshi Takagi, Koichiro Hattori, Yutaka Seino and Hidetoshi Nakano
National Institute of Advanced Industrial Science and Technology, Japan

To investigate the influence of geometric error of indenter tip in nano-indentation test, direct measurement of indenters and analyses of indentation process are carried out. Geometry of indenter tip is measured with a scanning probe microscope and geometrical parameters such as face angles, tip radius and truncation length are calculated. Based on these results, the models for the finite element analyses are created. Analyses of indentation processes into a metal sample are carried out and the influence of tip geometry is discussed.

Introduction

The geometry of indenter tip is one of the most significant sources of uncertainty in nano-indentation hardness test. It is specified in ISO/DIS 14577 [1] that the indenter area function should be verified with either direct or indirect measurement. However the indirect measurement method does not bring reliable results necessarily because it relies on the estimated machine compliance and material properties. Recently scanning probe microscopes (SPMs) are widely used in laboratories and they are getting to be applied for direct verification of indenter [2].

On the other hand the difference of tip geometry causes the different shape of impression. And it may also cause the difference of load-depth curve. However, to investigate these effects by experiments there are some problems. The reason is that reliable measurement in nano-range (h < 200 nm) is quite difficult.

In this study direct measurement of indenter with an SPM was described and finite element analyses with blunt indenters were achieved to discuss the effects of indenter-tip geometry.

Direct measurement of indenter shape

Direct verification of indenter tip was carried out with SII SPA400 scanning probe microscope operated in AFM contact mode. An indenter held on a small metal block was put on the sample stage of 200 μm-range scanner of the SPM. Sensitivity and nonlinearity of this scanner are corrected with verification data of pitch standard samples. However creep of the scanner cannot be eliminated because there are not any feedback mechanisms. Concerning x- or y-axis, the verification data shows that the repeatability in single scan line is within 3% and that in single frame does not exceed 10%. On z-axis, at least the same amount of uncertainty should be taken into consideration, although it is difficult to verify characteristics of scanner completely. Therefore the result of inspection should be reviewed with considering the uncertainty discussed above.

Berkovich pyramidal diamond indenters for ELIONIX ENT-1100a Nano Indentation Tester were inspected. Perspective views of indenters are illustrated in Fig. 1 and 2. Two figures represent a brand-new one and a used one, respectively. Even though an indenter is brand-new, the tip is already rounded and its radius and truncation (shown on Table 2) are not negligible. On an indenter after a number of indentations, the roundness is greater than that of a brand-new one and its radius and truncation are almost double. Because the surface of used indenter was smooth, this transformation seems to be caused by wear during repeated use. Any traces of cleavage were not observed on the surface of any indenters. The face angles can be calculated with direction cosines of regression planes of the faces of pyramid, regarding the composite vector of normal vectors of three faces as the axis of indenter. The

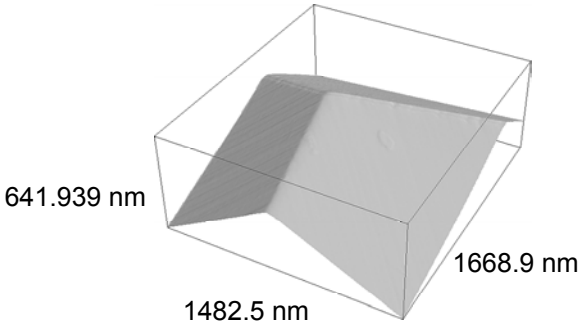

Fig. 1 SPM image of a brand-new indenter.

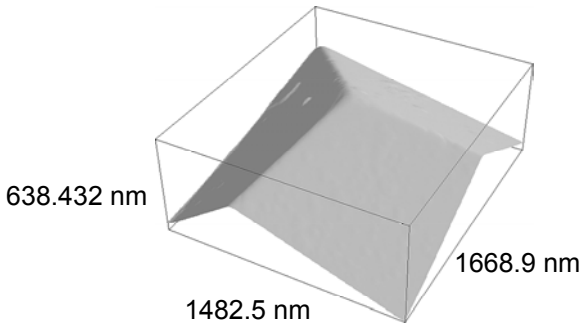

Fig. 2 SPM image of a used indenter.

results for a brand-new indenter and used one are listed in Table 1. These results show both indenters are sharper than ideal one (values of α are greater than 65.27 degrees). However it can be caused by the uncertainty of the SPM. In fact, all indenters we inspected showed the same tendency.

Fig. 3 shows a typical relationship between indentation depth and square root of projected or surface area (area function). If we consider that the area function for projected area can be expressed as [3]

$$A_P(h)=C_0\,(h-\Delta h)^2\,, \qquad (1)$$

the truncation of indenter can be obtained as a parameter Δh of the regression curve. Parameters for the indenters shown in Fig. 1 and 2 are listed in Table 2. Tip radii in this table were calculated based on the model described below [3]. According to SPM images of indenters, it is found that edges of pyramid are also rounded. Because the effect of edge roundness is not considered in equation (1), obtained truncation length may be overestimated.

If the area of truncated edges is assumed to be constant, equation (1) is modified to the form

$$A_P(h)=C_0\,(h-\Delta h)^2+3A_t, \qquad (2)$$

where A_t is the constant representing the truncated area of single edge. The parameters can be obtained by solving nonlinear equations of the method of least square using Newton-Raphson method.

Table 1 Examples of calculated face angles c

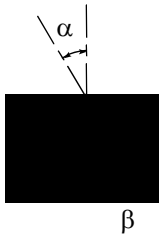

Symbol	Specified value [º]	Face No.	Angle [º] Brand-new	Used
α	65.27± 0.3 1)	1	64.3750	64.4061
		2	65.3329	66.4906
		3	62.3860	63.4549
		Ave.	64.0313	64.7839
β	60± 0.3 1)	1	66.0789	64.9333
		2	58.5290	61.1149
		3	55.3921	53.9518
θ	115± 0.25 2)	1	109.734	108.241
		2	120.658	120.053
		3	113.457	116.539
		Ave.	114.616	114.945

1) ISO/DIS 14577-2.2
2) Product specification (Tokyo Diamond Tool

Table 2 Estimation of truncation length and tip radius.

Indenter	Truncation length Δh [nm]	Effective radius R_{eff} [nm]
Brand-new	12.6467	436.237
Used	26.7600	1022.98

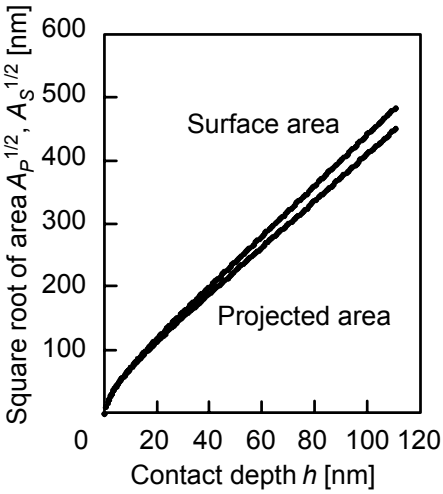

Fig. 3 An example of calculated area functions.

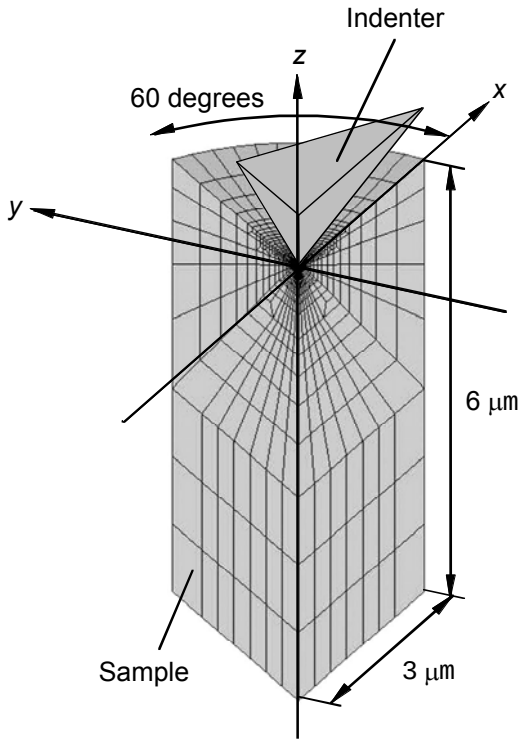

Fig. 4 The Finete element model.

Finite element analyses of indentations

To investigate the effects of indenter shape, finite element analyses were carried out. The model used for these calculations is illustrated in Fig. 4. Indentation into the center of the cylindrical region in the sample with diameter of 6 μm and depth of 6 μm was considered. Assuming the symmetry of triangular pyramid, 1/6 of this region was divided into finite elements. Therefore a cross section of the region was directed to an edge of pyramid and another cross section was directed to the center of a face of pyramid. 20-node hexahedral elements were used for this model. The element size just beneath the indenter tip was 10 nm so that it became small enough to the size of rounded area of indenter. Assuming the indenter to be a rigid body, the sample was assumed to be an elastoplastic body that was characterized by a bilinear isotropic hardening constitutive equation [4]. Material of the sample was chosen from metals of which properties are clearly known. Material properties for the sample are listed in Table 3 [5]. A model of blunt indenter was created by overlapping a triangular pyramid and a sphere. Its shape illustrated in Fig. 5 is specified by only one parameter, tip radius. Indentation cycle of loading and unloading was simulated, of which maximum penetration was up to 200 nm. The calculation was carried out by ANSYS Rev. 5.7. on IBM RS/6000 SP system at Tsukuba Advanced Computing Center, Institute of Advanced Industrial Science and Technology.

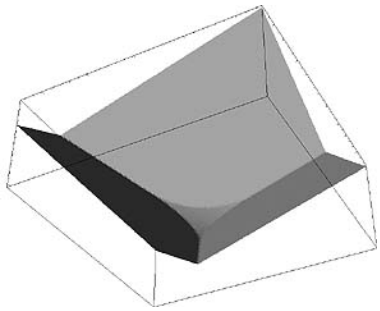

Fig. 5 A model of rounded indenter.

Table 3 Material properties.

Young's modulus [GPa]	Poisson's ratio	Yield stress [MPa]	Tangent ratio [MPa]
206	0.3	245	520

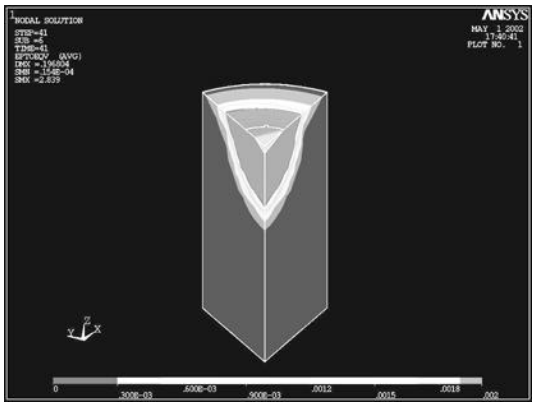

Fig. 6 Distribution of equivalent strain after 200 nm of penetration (whole region).

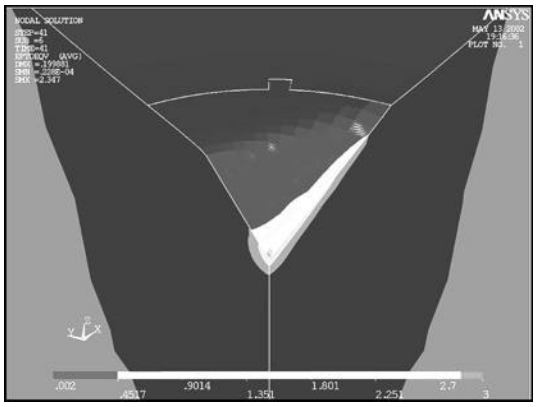

Fig. 7 Distribution of equivalent strain after 200 nm of penetration (close-up around an impression).

Results and discussions

Graphics of the results are shown in Fig. 6 and 7. Fig. 6 shows the distribution of total equivalent strain drawn on the deformed shape at penetration depth of 200 nm. The contour closest to the impression indicates 0.2% of total strain which corresponds to the region of plastic deformation. This region is enough distant from the boundary of the model. Therefore the result is assumed not to be influenced by the boundary. Fig. 7 shows the distribution of total equivalent strain around an impression with the ideal indenter. In all analyses, the strain is concentrated on an edge of pyramid. In case of the ideal indenter, the maximum strain appeared at the center of impression and meanwhile in case of a blunt indenter it appeared at the point where an edge of pyramid and a sphere are connected. Although total load is greater than that for the ideal indenter, maximum strain is lesser.

Fig. 8 shows load-depth curves for the ideal indenter and blunt indenters (loading parts of curves under 90 nm of penetration depth were shown). A distinctive feature of the curve for the ideal indenter is that the curve starts parallel with the horizontal axis at the origin. The result for the ideal indenter can be approximated well by quadratic equation (a solid line following the marks of calculated values for the ideal indenter). It means that the curve for the ideal indenter closely corresponds to the area function for the ideal indenter. For blunt indenters loads are greater than that of the ideal one and the load becomes greater as their tip radius is getting larger. Solid lines following the marks for the blunt indenters are quadratic curves created moving the regression curves for the ideal indenter horizontally by truncated length of the blunt indenters. These lines are coincident with the calculated value. That means the load is mainly dominated by area function of indenter. This conclusion may be effective when the material is relatively soft such as metals.

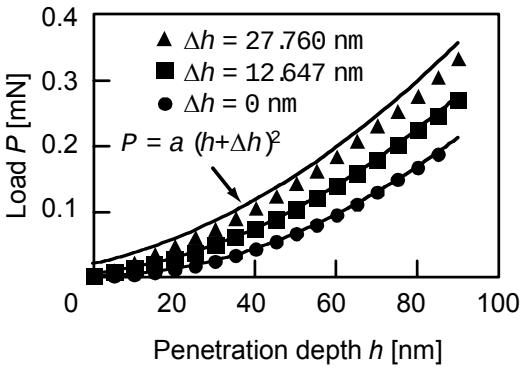

Fig. 8 Load-depth curves for indenters with various truncation length.

Conclusions

The shapes of indenters for nano-indentation were measured directly by an SPM and their geometric parameters were calculated. Even on a brand-new indenter the roundness of tip

was not negligible.

Indentation behaviors were analyzed with FEM and the relationship between indenter tip radii and load-depth curves was investigated. In case of relatively soft materials the load-displacement curve was dominated by area function of each indenter.

Refereces

[1] ISO/DIS 14577-2.2, International Organization for Standardization (2001)
[2] K. Hermann, F. Pohlenz, R. Seemann, K. Hasche, *Proc. 2nd euspen Int. Conf.* (2001) 436.
[3] A. Shimanoto, K. Tanaka, Y. Akiyama, H. Yoshizaki, *Phil. Mag. A*, **74** (1996) 1097.
[4] ANSYS Structural Analysis Guide, Ch. 8.
[5] ASM Handbook Vol. 8, ASM International.

Contact Point

Satoshi Takagi
Vibration and Hardness Section, Acoustics and Vibration Metrology Division
Metrology Institute of Japan,
National Institute of Advanced Industrial Science and Technology
AIST Tsukuba Central 3 1-1-1 Umezono Tsukuba Ibaraki 305-8563 Japan
e-Mail satoshi.takagi@aist.go.jp